Macromolecular Journals

Macromolecular Chemistry and Physics

Study of the Effects of Intramolecular and Intermolecular Hydrogen-Bonding Systems on the Polymerization of Amide-Containing Benzoxazines

Lu Han, Kan Zhang, Hatsuo Ishida,* Pablo Froimowicz*

Pure *para* and *ortho* position amide benzoxazines, ***p*HBA-a** and ***o*HBA-a**, are synthesized. The hydrogen bonding interactions occurring in ***p*HBA-a** and ***o*HBA-a** are studied by Fourier transform infrared (FT-IR) spectroscopy and proton nuclear magnetic resonance (^{1}H NMR) spectroscopy. FT-IR results show that, while ***p*HBA-a** presents intermolecular hydrogen bonding interactions, ***o*HBA-a** exhibits an intramolecular five-membered-ring hydrogen-bonding system between the NH in the amide group and the oxygen in the oxazine ring. Differential scanning calorimetry (DSC) is used to study the thermal properties of the resins and their respective polymers. A deeper understanding of the hydrogen bond interactions in this family of resins is attempted to have better insights on how these systems influence the polymerization behavior not only with respect to the polymerization temperature but also with respect to the propagation step.

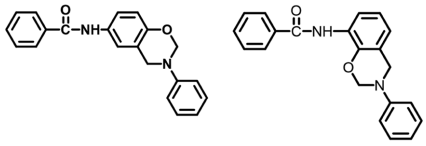

***p*HBA-a** ***o*HBA-a**

1. Introduction

Polybenzoxazine is a new category of thermoset materials that has been extensively studied in recent years due to the easy synthesis and outstanding properties.[1–3]

L. Han, Prof. H. Ishida
Department of Macromolecular Science and Engineering
Case Western Reserve University
Cleveland, OH 44106, USA
E-mail: hxi3@cwru.edu
Dr. K. Zhang
School of Materials Science and Engineering
Jiangsu University
Zhenjiang 212013, China
Prof. P. Froimowicz
Design and Chemistry of Macromolecules Group
Institute of Technology in Polymers and Nanotechnology (ITPN)
UBA-CONICET, School of Engineering
University of Buenos Aires
Av. Gral. Las Heras 2214
PC 1127AAR Buenos Aires, Argentina
E-mail: pxf106@case.edu

Benzoxazines can be synthesized by Mannich condensation from phenol, amine, and formaldehyde.[4] There are no reaction by-products formed during the cationic ring-opening polymerization. Benzoxazines possess an extremely rich molecular design flexibility making possible for benzoxazines to satisfy different applications due to the multiple choices of phenols, amines, and aldehyde.[5–7] The resulting polybenzoxazines show many unique properties such as near-zero volume changes upon polymerization,[8,9] low water absorption,[9] variable range of glass transition temperature,[10,11] fast physical and mechanical properties development at low conversion, and high char yield.[12,13] One additional advantage of polybenzoxazines is its good and easy compatibility with other polymers, thus enhancing the final properties of the obtained materials.[14–16]

Benzoxazine resins exhibit various unusual and often advantageous properties. One example is that most *ortho*-substituted benzoxazines show enhanced properties when compared to *para* position counterpart. In 2014, Liu and coworkers first demonstrated that the double *ortho*-substituted bisphenol F-based polybenzoxazines showed the

glass transition temperature (T_g) in the following order: *o*-,*o*- > *o*-,*p*- > *p*-,*p*- isomers. $\Delta T_g = T_{g,o\text{-},o\text{-}} - T_{g,\ p\text{-},p\text{-}}$ is 60 °C, which is completely opposite trend of all the literature examples of the *ortho* and *para* isomer studies reported. Apart from this, the *ortho*-substituted benzoxazines show the best thermal stability among all the isomers.[17] Later, Zhang and co-workers found that the *ortho*-amide-imide functional benzoxazine and *ortho*-norbornene functional benzoxazine monomers showed milder synthesis condition (shorter reaction time with high yield) as compared to *para* counterpart. Furthermore, the corresponding *ortho*-functionalized polymer showed higher T_g.[1,18,19]

Although a large number of benzoxazines have been synthesized to improve the physical and mechanical properties and the *ortho*-substituted functional benzoxazines show highly desirable properties, the fundamental reasons for the appearance of unexpected results are poorly understood. In our group's previous work, the synthesis of the ***p*HBA-a** and ***o*HBA-a** have been reported and a ring-opening and propagation mechanism for the *ortho* substituted isomer involving a five-membered-ring hydrogen bonding was proposed, which reveals how the intramolecular hydrogen bonding is influencing ring opening and chain propagation. Froimowicz *et al*. studied the isomeric benzoxazine system by solution NMR and demonstrated that the intramolecular hydrogen bonding does exist and that the 7-position on the benzene ring becomes more acidic and reactive than without hydrogen bonding.[20]

Para position benzoxazines are far less investigated in comparison to *ortho* position benzoxazines in their capability of forming hydrogen bonds. In this study, the hydrogen bonding behavior of two isomeric amide-containing benzoxazines, substituted at the *para* and *ortho* position, are studied by FT-IR. These results complement not only the long hypothesized existence of an intramolecular five-membered-ring hydrogen bond in ***o*HBA-a** proposed in previous papers[18,20] but also those more recently reported using NMR techniques.[3] It must be highlighted that to make this spectroscopic study fully reliable much emphasis has been paid on obtaining highly purified benzoxazine resins.

2. Experimental Section

2.1. Materials

o-Aminophenol (98%), *p*-aminophenol (98%), phenol (98%), benzoyl chloride, and paraformaldehyde (96%) were used as received from Sigma-Aldrich. Aniline was purchased from Aldrich and purified by distillation. **PH-a** was synthesized following reported methods.[21] Ethyl acetate, toluene, hexane, chloroform, 1,4-dioxane, sodium hydroxide (NaOH), lithium chloride (LiCl), and sodium sulfate were obtained from Fisher Scientific and used as received. 4-Methoxyphenol (99%) from Aldrich was recrystallized in ethyl acetate before use.

2.2. Sample Preparation

2.2.1. Synthesis of *N*-(2-Hydroxyphenyl)benzamide

o-Aminophenol (3.00 g, 27.5 mmol) and LiCl (1.15 g, 27.5 mmol) were dissolved in NMP (25 mL). The solution was cooled to 0 °C, and benzoyl chloride (3.88 g, 27.5 mmol) was added dropwise with a syringe. Then, the solution was kept at room temperature overnight. Next, the reaction mixture was poured into cold water. The precipitate was filtered and afterward dried under vacuum. Light pink crystals were obtained (yield 85%). ^{1}H NMR (600 MHz, DMSO-*d6*, δ): 6.77–7.95 (m, 9H, Ar*H*), 9.51 (s, 1H, N*H*), 9.74 (s, 1H, O*H*). FT-IR (KBr, cm^{-1}): 3408 (N—H stretching), 3029 (O—H stretching), 1645 (amide I), 747 (C=O bending).

2.2.2. Synthesis of *N*-(4-Hydroxyphenyl)benzamide

Exactly the same amounts and procedures as *N*-(2-hydroxyphenl) benzamide were used to synthesize *N*-(4-hydroxyphenl)-benzamide, except that *p*-aminophenol was used instead of *o*-aminophenol. The product was dried under vacuum to obtain a white powder (yield 82%). ^{1}H NMR (600 MHz, DMSO-*d6*, δ): 6.70–7.92 (m, 9H, Ar*H*), 9.25 (s, 1H, O*H*), 10.02 (s, 1H, N*H*). FT-IR (KBr, cm^{-1}): 3390 (O—H stretching), 3327 (N—H stretching), 1649 (amide I), and 720 (C=O bending).

2.2.3. Preparation of *N*-(3-Phenyl-3,4-dihydro-2*H*-benzo[e][1,3]oxazin-6-yl)benzamide (***p*HBA-a**)

Into a 50 mL round flask were added 20 mL of 1,4-dioxane, aniline (0.44 g, 4.70 mmol), *N*-(4-hydroxyphenyl)benzamide (1.00 g, 4.70 mmol), and paraformaldehyde (0.23 g, 9.40 mmol). The mixture was stirred at 100 °C for 24 h, and subsequently cooled to room temperature. Then the reaction mixture was poured into cold water (200 mL) to give a powder like precipitate. The product was dissolved in ethyl acetate and washed with 0.5 N NaOH solution and then water to eliminate the unreacted residual starting materials. The crude product was dried over anhydrous sodium sulfate followed by fractionating with column chromatography (eluent: hexanes and ethyl acetate, in a volume ratio of 3:1) to obtain the final product (yield 73%). ^{1}H NMR (600 MHz, DMSO-*d6*, δ): 4.64 (s, 2H, Ar—CH_2—N), 5.42 (s, 2H, O—CH_2—N), 6.70–7.91 (m, 13H, Ar*H*), and 10.07 (s, 1H, N*H*). FT-IR (KBr), cm^{-1}: 1646 (amide I), 1227 (C—O—C asymmetric stretching), and 940 (oxazine related band). Elemental analysis: calcd. for $C_{21}H_{18}N_2O_2$: C, 76.34%; H, 5.49%; and N, 8.48%; found: 75.44%; H, 5.23%; and N, 8.33%.

2.2.4. Preparation of *N*-(3-Phenyl-3,4-dihydro-2*H*-benzo[e][1,3]oxazin-8-yl)benzamide (***o*HBA-a**)

Into a 50 mL round flask were added 20 mL of chloroform, aniline (0.44 g, 4.70 mmol), *N*-(2-hydroxyphenyl) benzamide (1.00 g, 4.70 mmol), and paraformaldehyde (0.23 g, 9.40 mmol). The mixture was stirred at 80 °C for 24 h, and subsequently cooled to room temperature. Then, the solution was washed with cold water. The chloroform solution was dried over anhydrous

Macromol. Chem. Phys. **2017**, DOI: 10.1002/macp.201600562

sodium sulfate to obtain the crude product. The crude product was fractionated by column chromatography (eluent: hexanes and ethyl acetate, in a volume ratio of 3:1) to obtain pure final product (yield 80%). ^{1}H NMR (600 MHz, DMSO-*d6*, δ): 4.67 (s, 2H, Ar-C*H*$_2$—N), 5.51 (s, 2H, O—C*H*$_2$—N), 6.87–7.94 (m, 13H, Ar*H*), 9.35 (s, 1H, N*H*). IR spectra (KBr), cm^{-1}: 1666 (amide I), 1237 (C—O—C asymmetric stretching), and 921 (oxazine related). Elemental analysis: calcd. for $C_{21}H_{18}N_2O_2$: C, 76.34%; H, 5.49%; and N, 8.48%; found: 75.96%; H, 5.34%; and N, 8.41%.

2.3. FT-IR Characterization

PH-a, *p*HBA-a, and ***o*HBA** were studied by solution FT-IR in a liquid cell. The optical crystals are made of thallium bromo iodide (KRS-5). The average pathlength is 0.539 mm, which is the actual cell pathlength calculated from the interference fringe of the empty cell. To minimize possible interference caused by water, moisture, and humidity, chloroform was kept over activated molecular sieves overnight and distilled at boiling temperature. The distilled chloroform was collected and ready for preparing the different solution at the proper concentrations for each compound, **PH-a, *p*HBA-a**, and ***o*HBA**. The compounds were also dried and kept in a vacuum oven for 2 days to eliminate water.

***p*HBA-a** and ***o*HBA-a** were dissolved in chloroform at the following concentrations: 1.0, 1.9, 3.0, 3.8, 10.0, 19.0, 30.0, and 38.0 $\times$ 10^{-3} M. During the process of dissolving the compounds, it was found that ***o*HBA-a** was the easiest to dissolve, whereas ***p*HBA-a** took longer to dissolve in chloroform. The compounds were dissolved completely without any heating procedure which might potentially disrupt the natural arrange or hydrogen bonding system. Such care is important as hydrogen bonding structure is the focus of this study.

A Bomem Michelson MB100 FT-IR spectrometer equipped with a deuterated triglycine sulfate detector and a dry air purge unit was used to carry out this study. Sixty-four scans were coadded at the resolution of 4 cm^{-1}. The frequency of a band was determined after 11th polynomial curve fitting and interpolation of the data points.

2.4. NMR Characterization

^{1}H and ^{13}C NMR spectra were recorded on a Varian Oxford AS600 NMR spectrometer at the proton frequency of 600 MHz and its corresponding carbon frequency of 150.864 MHz using trimethylsilane as an internal standard. The parameters for the NMR acquisitions are: 64 scans for ^{1}H NMR and 1024 scans for ^{13}C NMR, and room temperature data collection. For quantitative intensity data collection, a relaxation time of 10 s was used for ^{1}H NMR spectral measurements. Concentration of the samples were 10 mg of compound/0.8 mL of solvent unless otherwise mentioned.

3. Results and Discussion

3.1. Synthesis

The successful synthesis of amide monofunctional benzoxazine monomers was achieved using primary amine (aniline), paraformaldehyde, and amide functional phenols (*para* and *ortho* isomers) as well as phenol, as indicated in Scheme 1 and Figure 1. The monomers are designated as ***p*HBA-a** and ***o*HBA-a** in which the small letters in italic represent the

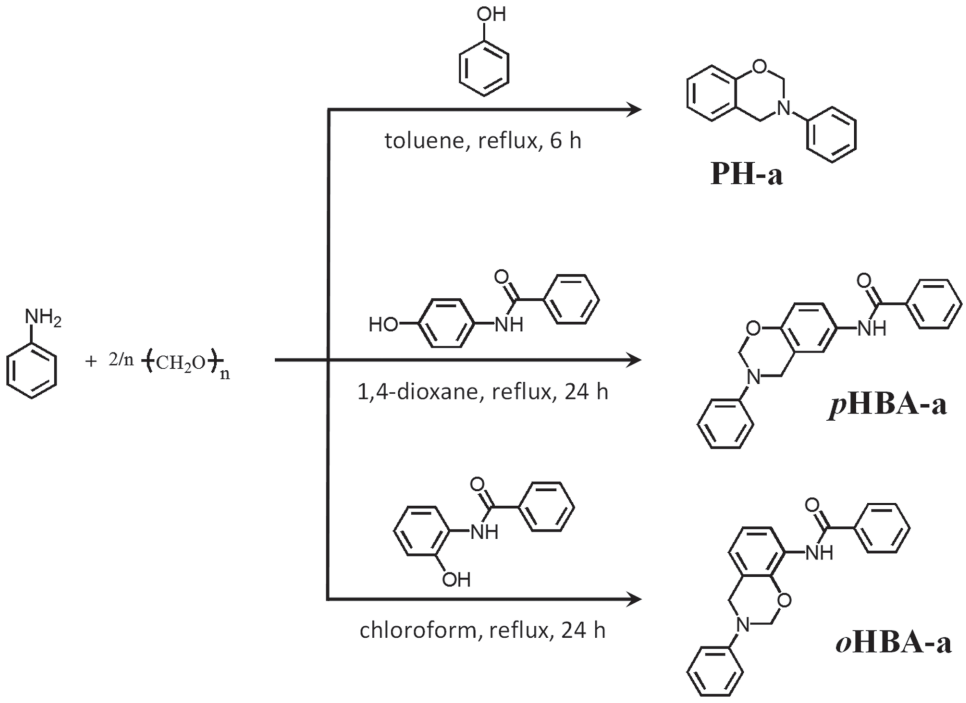

Scheme 1. Synthesis of benzoxazine monomers **PH-a**, ***p*HBA-a**, and ***o*HBA-a**.

position of the amide group either at the *para* or *ortho* position with respect to the oxygen atom in the oxazine ring. The reaction condition for ***p*HBA-a** is harsher than ***o*HBA-a**: 1,4-dioxane as a solvent allows a higher reaction temperature, which increases the solubility of the reactants. The reason that a polar solvent is favored for ***p*HBA-a** is probably because the hydroxyl group on the *para* position of the amide group is exposed to interact favorably with the hydrophilic solvent. There is no possibility for the formation of the intramolecular hydrogen bonding between oxygen atom and NH in amide group when the NH group is in the *para* position with respect to the oxygen atom of the oxazine ring. **PH-a** represents a phenol/aniline type monofunctional benzoxazine monomer synthesized with no amide group in the structure. Its synthesis is also presented in Scheme 1.

Previous study on ***p*HBA-a** and ***o*HBA-a** was focused on the monofunctional benzoxazines functioned as precursors when synthesizing polybenzoxazoles. The samples used for the study were not of the sufficient purity to minimize the interference from the impurities. Column chromatography and recrystallization after common synthesis were carried out to obtain highly pure material for the current study.

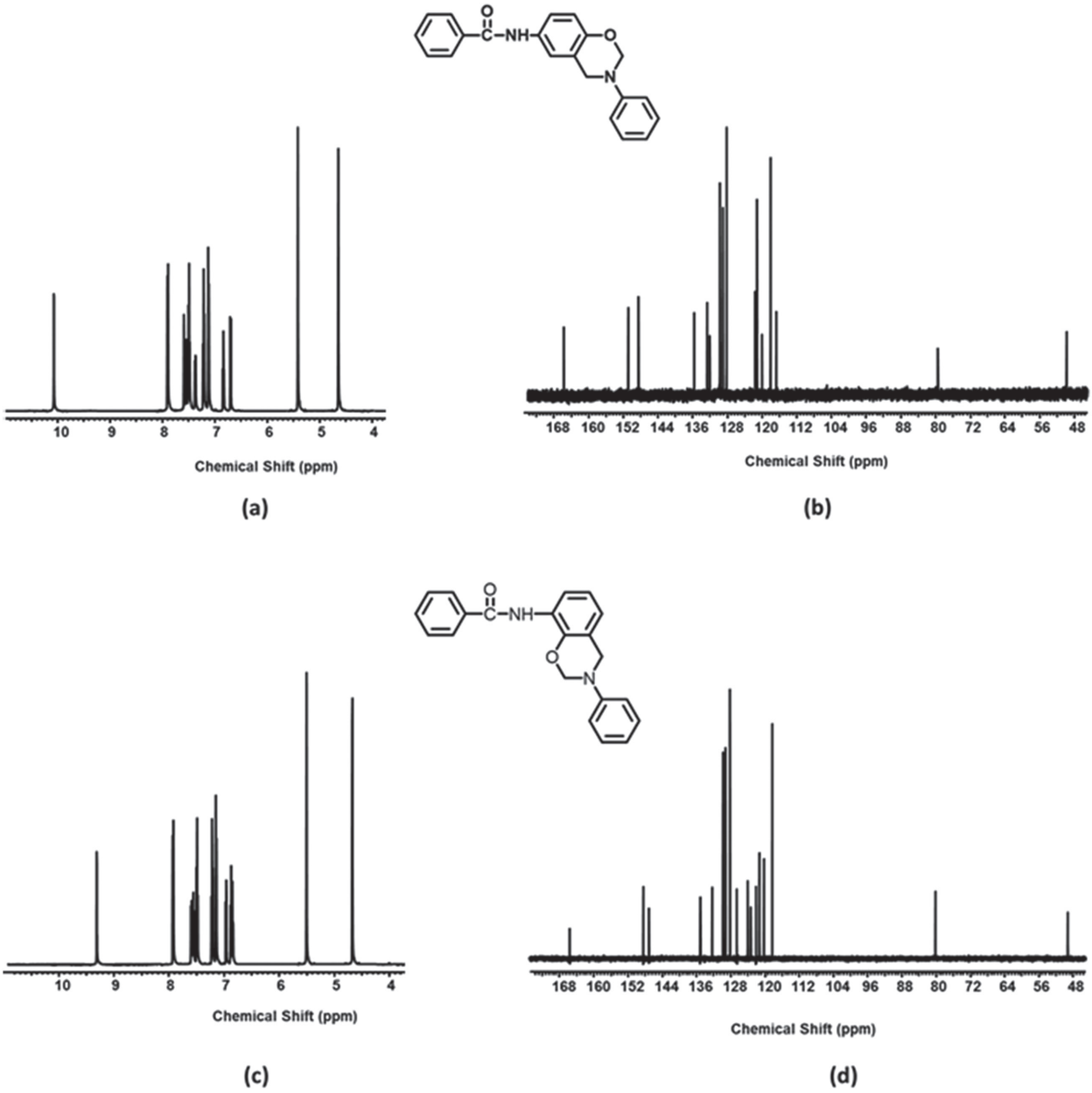

Figure 1. a) ^{1}H and b) ^{13}C NMR spectra of ***p*HBA-a**, c) ^{1}H and d) ^{13}C NMR spectra of ***o*HBA-a**.

Macromol. Chem. Phys. **2017**, DOI: 10.1002/macp.201600562

3.2. FT-IR Study

Intra- and intermolecular hydrogen bonding studies are most often carried out using carbon tetrachloride as the solvent of choice. One of the main reasons for this selection is that carbon tetrachloride is neither a hydrogen boning acceptor nor a donor. Additionally, this solvent presents a rather low polarity.[22,23] Therefore, extra interactions with, or caused by, the solvent are eliminated and all spectroscopic information can be assumed to be from system under study. Also, this molecule exhibits no interfering band in the spectral region of interest between 4000 and 2000 cm^{-1}. Taking into consideration that if two or more molecules are to be studied and compared, the conditions for the study must ideally be kept identical. Solubility tests of the two isomeric compounds in carbon tetrachloride (CCl_4) revealed that one of the isomers, ***o*HBA-a**, exhibited a good solubility, whereas the other one, ***p*HBA-a**, a very poor one in the same solvent within the desired concentration ranges. The main reason for this difference is related to the solvation capability of the solvent (CCl_4) toward each isomeric molecule. ***o*HBA-a** bears an intramolecular hydrogen bond within its molecular structure and no intermolecular ones. This favors its solvation and solubilization in CCl_4 since there seems to be no important connectivity between different molecules of the same compound. On the contrary, ***p*HBA-a** forms intermolecular hydrogen bonds, thus establishing interactions between different molecules of the same ***p*HBA-a**. As these interactions between molecules of ***p*HBA-a** are stronger than those existing between the solvent (CCl_4) and ***p*HBA-a**, ***p*HBA-a** cannot be easily solvated nor totally dissolved in this solvent. Formation of aggregate *via* hydrogen bonding might also occur in these conditions,[24] thus interfering with the measurements. These experimental results do not permit to prepare a set of solutions covering the very same concentration range for each isomer, thus making impossible to have identical conditions for the study and losing therefore comparability. In consequence, carbon tetrachloride was replaced by chloroform as the solvent due to the better solubility of the two compounds in it albeit the possibility of an interaction between the solvent and solute. This change in the solvent has been reported for other systems.[25]

FT-IR spectra at different concentrations of the two isomeric compounds were collected covering the concentration range between 1 and 38×10^{-3} M. The shift observed for the maximum of the N—H stretching band, summarized in Table 1, was used for the hydrogen bonding study.

3.2.1. **PH-a**

This compound was not studied in solution since there is no hydrogen bonding to be analyzed.

3.2.2. ***p*HBA-a**

The N—H stretching mode responded to concentration change in an unexpected way. The ***p*HBA-a** N—H stretching frequency changes with concentration change. However, increasing the concentration, the band position increases. This blue shifting caused by increasing the concentration is known as improper hydrogen bonding. The change indicates that, in the case of ***p*HBA-a**, there might be another hydrogen bonding, most likely weak and influenced by the concentration. The half width at half height of the N—H stretching mode shown in Figure 2 is broad and the positions are typical for hydrogen bonded N—H stretching region, indicating the absence of free N—H stretching mode.

3.2.3. ***p*HBA-a**

***o*HBA-a** shows intramolecular hydrogen bonding behavior which can be concluded from the relatively constant peak

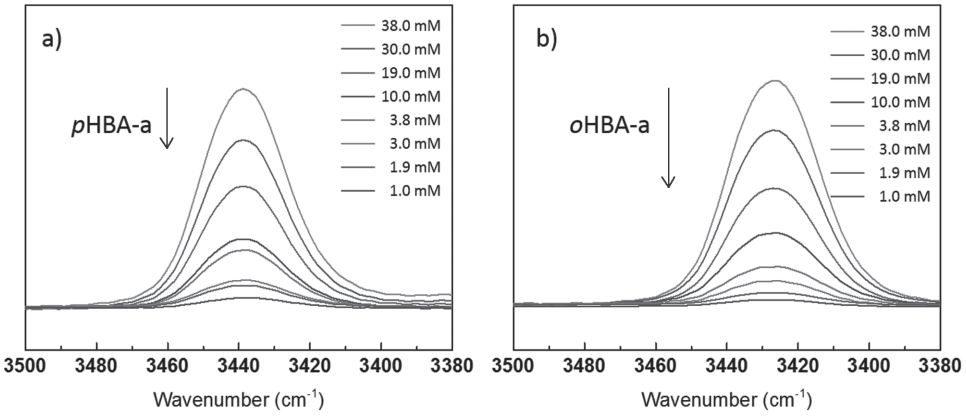

Figure 2. FT-IR spectra showing the region between 3500 and 3380 cm^{-1} for a) ***p*HBA-a** and b) ***o*HBA-a**. Spectra were recorded in solution at different concentrations using $CHCl_3$ as solvent.

Table 1. Maxima of the N—H stretching absorption bands observed by FT-IR. Spectra were recorded in solution using $CHCl_3$ as a solvent.

Concentration $\times 10^{-3}$ M	Wavenumber [cm^{-1}]	
	***p*HBA-a**	***o*HBA-a**
1.0	3436.46	3427.08
1.9	3437.45	3426.96
3.0	3437.81	3426.70
3.8	3438.36	3426.71
10.0	3438.76	3426.23
19.0	3438.77	3426.79
30.0	3438.84	3426.79
38.0	3438.80	3426.54

position within the concentration range studied. More importantly, the N—H position redshifted to around 3426.7 cm^{-1} compare to ***p*HBA-a**, the $\Delta_{\text{wave number}}$ is 12.2 cm^{-1}, which is consistent with intramolecular hydrogen bonding behavior of ***o*HBA-a** since intramolecular hydrogen bonding is typically stronger than the intermolecular hydrogen bonding.

Figure 3 indicates that, with the increase on the concentration, the maximum of the N—H stretching band of ***p*HBA-a** shifts to higher wavenumbers. The change, although in a small magnitude, perfectly follows a well-defined tendency. This behavior is related to intermolecular hydrogen bonding. In the case of ***o*HBA-a**, however, the maximum of the same N—H stretching band remains at the very same value with the concentration changes, which is characteristic for intramolecular hydrogen bonding. Intramolecular hydrogen bonding is formed between the N—H in amide group and the O in oxazine ring. No matter how low the concentration is, the

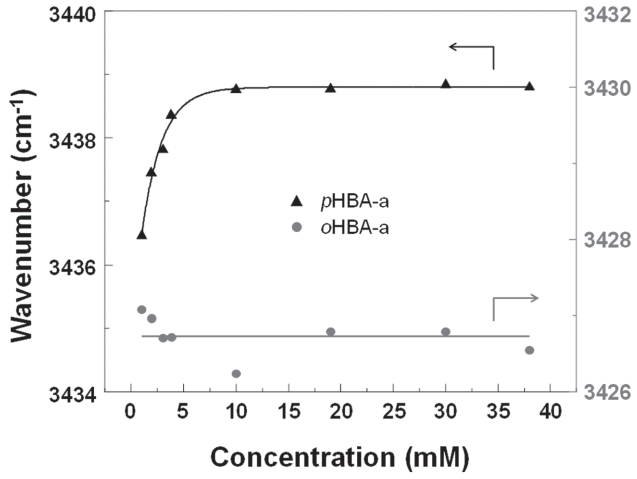

Figure 3. ***p*HBA-a** and ***o*HBA-a** N—H stretching wavenumber *versus* concentration.

frequency stays unaltered thus suggesting the presence of the mentioned intramolecular hydrogen bonding.

Extensive previous studies have been done on the hydrogen bonding of secondary amides. FT-IR is a powerful tool to study hydrogen bonding as the frequency is very sensitive to the strength of hydrogen bonds and pattern of the shift representative to the mode of hydrogen bonding.[26,27] Free N—H hydrogen bonding is characterized by the wavenumber in the range of 3500–3400 cm^{-1}. The free N—H stretching mode of N-methylacetamide, the simplest secondary amide model compound, in the vapor phase, was reported to be of 3472 cm^{-1}. The position of the N—H stretching band is in the range of intermolecular hydrogen bonding region. The standard intermolecular hydrogen bonded amide-amide (C=O···H—N), appears in the range between 3370 to 3250 cm^{-1}.[28] A specific frequency of the N—H stretching mode depends on the molecular structure of amide compound, type of solvent used, and temperature (see Table 2). Thus, weak interactions will also influence the position. The peak position can shift due to interaction with the solvent from 3452 cm^{-1} in chloroform to 3442 cm^{-1} in C_6H_6, the latter one is influenced by N—H···π hydrogen bonding interactions. The steric hindrance also affects the N—H stretching band position.

It can be observed in Figure 3 that ***p*HBA-a** showed an unexpected hydrogen bonding behavior. With the increase of concentration, ***p*HBA-a** N—H hydrogen bonding maxima position blueshifted to higher wavenumbers. It is worth noticing that the profile observed with the increase in concentration is asymptotic, whose maximum value at the plateau frequency of 3439 cm^{-1} is reached at concentration of $\approx 10 \times 10^{-3}$ M.

3.3. NMR Study

A detailed work on ***o*HBA-a** by different NMR techniques has recently been reported by our group.[20] However, much less attention has been paid to the ***p*HBA-a** isomer. In this section, we focus on this isomer complementing not only the reported work on NMR but also the FT-IR studies presented in the previous section. Figure 4 shows ^{1}H NMR spectra of ***p*HBA-a** at different concentrations.

It is known that for a reaction between two species to happen both species should be sufficiently activated. The cases presented in this study evaluate a single compound reacting with itself. Under these conditions, the compound should then present at least two different positions appropriately and sufficiently activated to be able to react. In this regard, compounds ***o*HBA-a** and ***p*HBA-a** were recently studied. This article reported on how the different positions on the anilide ring were activated.[20] Indeed, it was shown that the activation was more effective in ***o*HBA-a**, followed by ***p*HBA-a**, and then **PH-a**. At this stage, the ^{1}H NMR spectra of each benzoxazine

Macromol. Chem. Phys. **2017**, DOI: 10.1002/macp.201600562

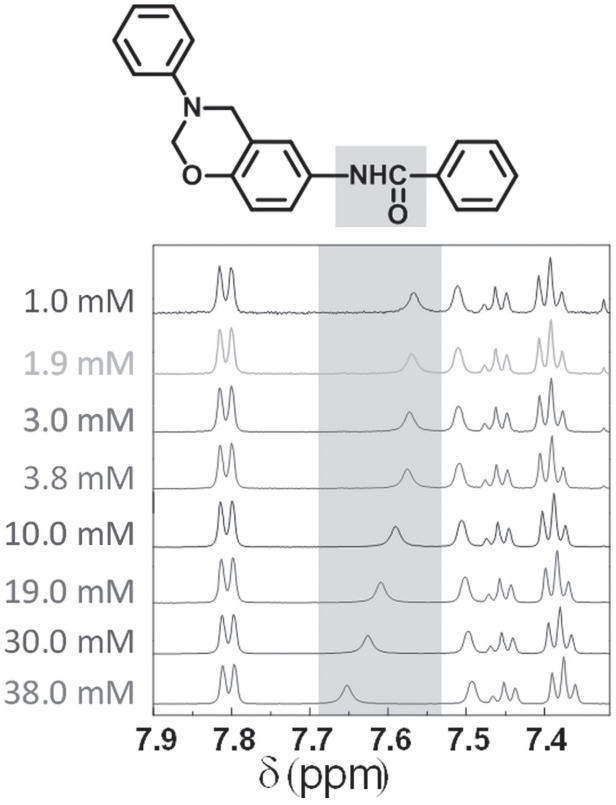

Figure 4. ^{1}H NMR spectra of ***p*HBA-a** at different concentrations. All spectra were recorded at 25 °C using $CDCl_3$ as a solvent.

were analyzed to estimate the reactivity but now at the 2-position. Table 3 shows the chemical shifts of those $-O-CH_2-N=$, and the respective $=N-CH_2-Ar$ to be taken as internal references, using DMSO-d_6 and $CDCl_3$ as solvents.

Table 2. Examples of reported results on secondary amide N–H stretching band positions determined by FT-IR.[29]

Chemical structure	Solvent	Concentration $\times 10^{-3}$ M	N–H Stretching peak position [cm^{-1}]
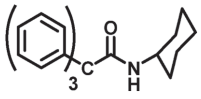	$CHCl_3$	10	3424
	DMSO	10	3298 (major) 3426 (minor)
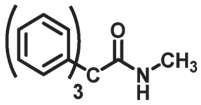	$CHCl_3$	10	3449
	DMSO	10	3315 (major) 3449 (minor)

In both solvents, the $\Delta\delta$ is greater for ***o*HBA-a** than for the other two resins. As has been reported, however, DMSO-d_6 has a high polarity and a strong capability to act as a hydrogen-bond acceptor. Thus, DMSO-d_6 compete and disrupt the intramolecular hydrogen bonds in ***o*HBA-a**, possibly forming intermolecular ones with the solvent. This may be the very reason for this decreased difference between the $\Delta\delta$ in $CDCl_3$ compared to the $\Delta\delta$ in DMSO-d_6. In contrast, as $CDCl_3$ is a low polar solvent, behavior in this solvent might be closer to what is experienced by benzoxazines when reacting, except by the understandable dilution. As can be seen in Table 3, the reference protons from the $=N-CH_2-Ar$ of the three resins show frequencies practically at the same chemical shifts. Nevertheless, the results are different for the frequency corresponding to $-O-CH_2-N=$. While resins **PH-a** and ***p*HBA-a** present the peaks at very similar frequencies, in ***o*HBA-a,** the peak is shifted toward greater δ (downfield). Thus, the $-O-CH_2-N=$ of ***o*HBA-a** are a little more acidic than those of the other two resins. This could in turn be interpreted as ***o*HBA-a** having this particular position a little more activated. Once again, ***o*HBA-a** shows a higher reactivity not only in its anilide positions but also in its 2-position. This is in agreement to its higher reactivity toward polymerization as experimentally observed by differential scanning calorimetry (DSC). Thus, given the thermal conditions, positions from the anilide could directly attack the more activated 2-position in ***o*HBA-a**, thus initiating the polymerization, as has been suggested in previous studies.[20] Finally, it must be mentioned that, in terms of reactivity, ***p*HBA-a** is in an intermediate situation between **PH-a** and ***o*HBA-a**. Consequently, the initiation mechanism(s) that ***p*HBA-a** could undergo will depend on the specific conditions.

3.4. Thermal Behavior Study

DSC was used to study the thermal behavior of each resin. Thus, Figure 5 shows the thermograms of each benzoxazine monomer, ***o*HBA-a** and ***p*HBA-a**, as well as the unsubstituted **PH-a**.

As can be seen in the figure, **PH-a** shows a sharp melting endotherm centered at 58 °C, which at the same time is highly symmetric. This aspect ratio for the melting of crystals is characteristic for compounds exhibiting high purity. In fact, melting point is often used in organic chemistry as a simple although efficient purity criterion.

Similarly, ***p*HBA-a** shows a sharp and highly symmetric endothermic peak at 151 °C, also indicating high purity for this benzoxazine resin. In the case of ***o*HBA-a,** a more complex situation is observed, where a nicely defined endothermic peak centered at 116 °C is first observed, followed by a very small, highly overlapped exothermic

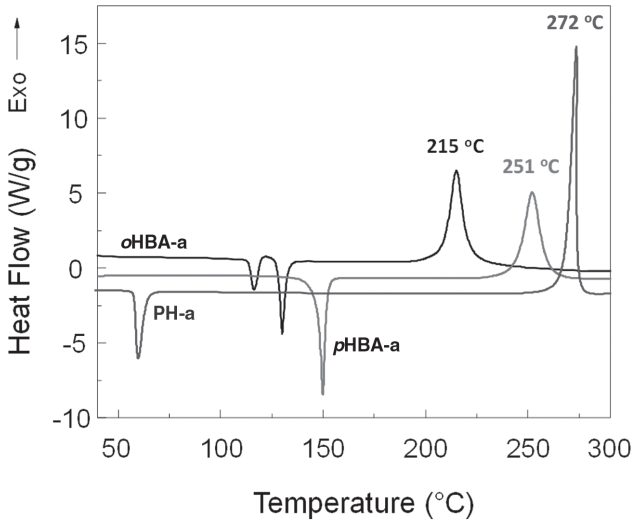

Figure 5. DSC thermograms comparing ***o*HBA-a** and ***p*HBA-a** with **PH-a**.

peak at 122 °C, which is then followed by a new endothermic peak centered at 130 °C. This behavior is consistent with a previously reported crystal-to-crystal phase transition.[30,31] The crystal of ***o*HBA-a** might be recrystallized into another more stable crystal form during the first melting stage. However, the meaningful observation to pay attention here is that both melting endotherms, and especially the second one, which is a cleaner transition, are once again sharp and highly symmetric. This result also strongly supports the high purity achieved for ***o*HBA-a**.

As can be seen, **PH-a** exhibits the lowest melting point, followed by ***o*HBA-a** (including both melting points), and finally ***p*HBA-a** showing the highest one. The order in the melting temperatures of analogous compounds, or even isomers as is the cases for ***p*HBA-a** and ***o*HBA-a**, can also uncover molecular interactions. For instance, the intramolecular hydrogen bonds in ***o*HBA-a** interact within the molecule, whereas the intermolecular hydrogen bonds in ***p*HBA-a** interact between molecules. Thus, intermolecular hydrogen bonds result in a stronger driving force for crystal formation, generating higher melting temperature. As a result, ***o*HBA-a** exhibits a lower melting temperature than ***p*HBA-a**.

A similar rationalization can be applied based on the same hydrogen-bonding interaction, but now addressing this issue with the solubility exhibited by these two compounds, ***p*HBA-a** and ***o*HBA-a**. Understandably, ***o*HBA-a** has better and higher solubility than ***p*HBA-a** in most of the organic solvents.[20]

The thermal behavior of **PH-a**, ***p*HBA-a**, and ***o*HBA-a** toward polymerization was then studied by DSC as depicted in Figure 5. The thermogram of **PH-a** shows that this compound does polymerize despite its high purity. The exothermic peak assigned to polymerization has its maximum centered at 272 °C. It must be highlighted, however, that **PH-a** in this condition has polymerized at a noticeably much higher temperature than the usual temperatures reported for this compound, usually around 260 °C,[21] reflecting the higher purity of the **PH-a** used in this study as compared to those used for other reported papers. Similar to what has been observed for **PH-a**, ***p*HBA-a** and ***o*HBA-a** also showed exothermic peak associated with their polymerizations. Specifically, the peak maximum is centered at 251 and 215 °C for ***p*HBA-a** and ***o*HBA-a**, respectively. Summarizing, **PH-a** exhibits the highest polymerization temperature, followed by ***p*HBA-a**, and finally ***o*HBA-a** showing the lowest one of the three studied compounds. This behavior has in fact already been reported.[20] What is shown in this study, however, is that their polymerization temperatures are indeed affected, but the order in which they do even though their high purity is not altered.

A close look at Figure 5 evidences that compared to the exotherm seen for **PH-a**, ***o*HBA-a** is broader, and ***p*HBA-a** is the broadest one. Interestingly, the results obtained by DSC show that while both inter- and intramolecular hydrogen-bonding systems have an excellent acceleration effect to initiate the polymerization, they seem to somehow lower the rate of the propagation step on the crosslinking polymerization. The previous result strongly suggests that regardless of the polymerization temperature of these benzoxazines, the propagation step for each resin faces different conditions, although not necessarily different mechanisms. It has been reported that benzoxazine resin based on bisphenol A and aniline (**BA-a**) that is polymerized in hydrogen bond forming solvent (or blend partner) shows higher T_g than the values predicted by the Fox equation for the blend composition of these two materials.[32–39] A possible mechanism for this has also been reported which is the competition between the propagating species and hydrogen bonding environment.[40,41] A similar situation might exists in the current comparison of those three monomers, **PH-a, *o*HBA-a**, and ***p*HBA-a**. It can be seen that **PH-a** do not have hydrogen bond forming structures at the onset of polymerization, and ***o*HBA-a** to some extent of hydrogen forming species created by the weakening of the intramolecular hydrogen bonding at elevated temperature, and finally a large number of available hydrogen bonding species in ***p*HBA-a**. Thus, based on simply hydrogen bonding environment point of view, the extensive network formation improves in the order of **PH-a, *o*HBA-a**, and ***p*HBA-a**, which is different from the polymerization rate order of **PH-a**, ***p*HBA-a**, and ***o*HBA-a**.

Figure 6 shows the comparison of the DSC thermograms of three polymers obtained by polymerizing, for 2 h, the three resins at the onset temperature of their respective exotherm (according to Figure 5). The onset

Macromol. Chem. Phys. **2017**, DOI: 10.1002/macp.201600562

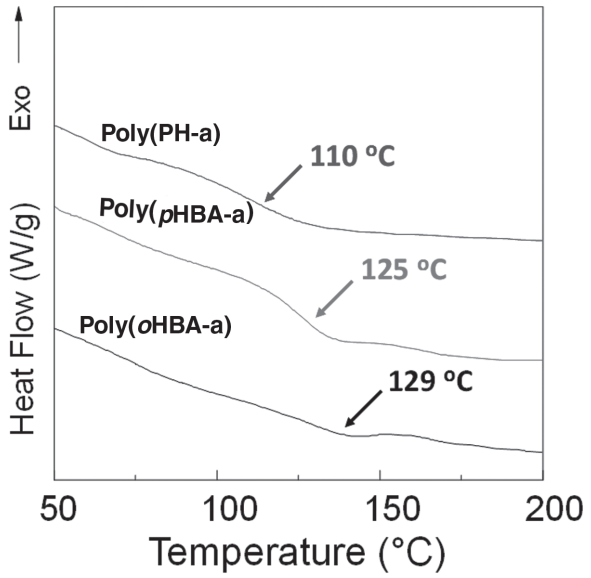

Figure 6. DSC thermograms comparing **poly(PH-a)**, **poly(*p*HBA-a)**, and **poly(*o*HBA-a)**.

temperatures are 260, 240, and 210 °C for **PH-a**, ***p*HBA-a**, and ***o*HBA-a**, respectively.

The result can be explained by the electronic effects we reported previously. The glass transition temperature (T_g) order for the obtained thermosets is as follows: **poly(*o*HBA-a)** > **poly(*p*HBA-a)** > **poly(PH-a),** which is in fact a reverse sequence of the polymerization temperature order of their precursors: **PH-a** > ***p*HBA-a** > ***o*HBA-a**. Thus, **PH-a** shows the highest polymerization temperature but the lowest T_g when compared to ***p*HBA-a** and ***o*HBA-a**. On the contrary, ***o*HBA-a** presents the lowest polymerization temperature and the highest T_g. Finally, ***p*HBA-a** exhibits temperatures between the other two compounds in both cases. It is interesting to note that the T_g difference between **poly(*p*HBA-a)** and **poly(*o*HBA-a)** is not as dramatic as the polymerization exotherm temperature difference might indicate. This might be due to the competing effect of the rate of polymerization and network formation as discussed above.

The previous results might be rationalized as follows: on the one hand, ***o*HBA-a** presents more reactive positions that are more activated than in the other two compounds in the aromatic ring adjacent to the oxazine moiety. Thus, initiation occurs at lower temperature. Moreover, the other activated positions in the same aromatic ring might simultaneously act as crosslinking points during the propagation step, thus generating the most cross-linked network. On the other hand, **PH-a** shows the highest polymerization temperature since this compound does not have any activating substituent in its structure. The only reactive positions in the aromatic ring adjacent to the oxazine moiety (the 6- and 8-positions, also called *para* and *ortho* positions) are intrinsically and slightly activated by the oxygen from the oxazine moiety inducing low crosslinking, thus obtaining the thermoset with the lowest T_g of the three studied systems. Finally, ***p*HBA-a** bears more reactive positions which are also more activated than in **PH-a**. However, when compared to ***o*HBA-a**, ***p*HBA-a** presents the same number of reactive positions but less activated. The intermediate reactivity of ***p*HBA-a** makes it more reactive than **PH-a** but less than ***o*HBA-a** in terms of initiation as well as in its crosslinking ability.

4. Conclusions

The hydrogen bond structure and its influence on the amide-containing benzoxazines ***p*HBA-a** and ***o*HBA-a** have been studied by FT-IR and ^{1}H NMR. The results have offered clear evidence for the existence of two different types of hydrogen-bonding systems, inter- and intramolecular hydrogen bonds. While ***p*HBA-a** exhibits an unexpectedly strong intermolecular hydrogen bonding behavior, which has made difficult its analysis in the past, results obtained for ***o*HBA-a** are in agreement with those supporting the intramolecular five-membered-ring hydrogen bonding.

Finally, it has been observed that the hydrogen bonding systems influence the benzoxazine polymerization behavior not only with respect to the polymerization

Table 3. Chemical shifts of the $-O-CH_2-N=$ and $=N-CH_2-Ar$ in $CDCl_3$ and DMSO-d_6 as a solvent.

Benzoxazine resin	$-O-CH_2-N=$ [ppm]		$=N-CH_2-Ar$ [ppm]		$\Delta\delta$[a)]	
	$CDCl_3$	DMSO-d_6	$CDCl_3$	DMSO-d_6	$CDCl_3$	DMSO-d_6
PH-a	5.35	5.42	4.63	4.63	0.72	0.79
***p*HBA-a**	5.37	5.42	4.66	4.64	0.71	0.78
***o*HBA-a**	5.47	5.51	4.65	4.67	0.82	0.84

a) $\Delta\delta = (\delta_{-O-CH_2N=}) - (\delta_{=N-CH_2-Ar})$.

temperature, but also and importantly, with respect to the propagation rates as well as crosslinking ability.

Received: November 28, 2016; Revised: January 3, 2017; Published online: ; DOI: 10.1002/macp.201600562

Keywords: benzoxazine; FT-IR; hydrogen bonding; NMR; polybenzoxazine

[1] K. Zhang, P. Froimowicz, L. Han, H Ishida, *J. Polym. Sci. Part A: Polym. Chem.* **2016**, *54*, 3635.
[2] S. Ohashi, V. Pandey, C. R. Arza, P. Froimowicz, H. Ishida, *Polym. Chem.* **2016**, *7*, 2245.
[3] W. Zhang, P. Froimowicz, C. R. Arza, S. Ohashi, Z. Xin, H. Ishida, *Macromolecules* **2016**, *49*, 7129.
[4] X. Ning, H. Ishida, *J. Polym. Sci. Part A: Polym. Chem.* **1994**, *32*, 1121.
[5] A. Chernykh, T. Agag, H. Ishida, *Polymer* **2009**, *50*, 382.
[6] P. Froimowicz, R. C. Arza, L. Han, H. Ishida, *ChemSusChem* **2016**, *9*, 1898.
[7] S. Ohashi, F. Cassidy, S. Huang, K. Chiou, H. Ishida, *Poly. Chem.* **2016**, *7*, 7177.
[8] H. Ishida, D. J. Allen, *J. Appl. Polym. Sci.* **2001**, *79*, 406.
[9] H. Ishida, D. J. Allen, *J. Polym. Sci. Part B: Polym. Phys.* **1996**, *34*, 1019.
[10] Y.-L. Liu, C.-I. Chou, *J. Polym. Sci. Part A: Polym. Chem.* **2005**, *43*, 5267.
[11] C. H. Lin, S. L. Chang, T. Y. Shen, Y. S. Shih, H. T. Lin, C. F. Wang, *Polym. Chem.* **2012**, *3*, 935.
[12] J. Si, P. Xu, W. He, S. Wang, X. Jing, *Composites Part A* **2012**, *43*, 2249.
[13] H. Qi, G. Pan, L. Yin, Y. Zhuang, F. Huang, L. Du, *J. Appl. Polym. Sci.* **2009**, *114*, 3026.
[14] N. Erden, S. C. Jana, *Macromol. Chem. Phys.* **2013**, *214*, 1225.
[15] Z. Fu, K. Xu, X. Liu, J. Wu, C. Tan, M. Chen, *Macromol. Chem. Phys.* **2013**, *214*, 1122.
[16] K. Chiou, E. Hollanger, T. Agag, H. Ishida, *Macromol. Chem. Phys.* **2013**, *214*, 1629.
[17] J. Liu, H. Ishida, *Macromol.* **2014**, *47*, 5682.
[18] K. Zhang, H. Ishida, *Front. Mater.* **2015**, *2*, 1.
[19] K. Zhang, J. Liu, S. Ohashi, X. Liu, Z. Han, H. Ishida, *J. Polym. Sci. Part A: Polym. Chem.* **2015**, *53*, 1330.
[20] P. Froimowicz, K. Zhang, H. Ishida, *Chem.— Eur. J.* **2016**, *22*, 2691.
[21] S. Ohashi, J. Kilbane, T. Heyl, H. Ishida, *Macromolecules* **2015**, *48*, 8412.
[22] J. L. Cook, C. A. Hunter, C. M. R. Low, A. Perez-Velasco, J. G. Vinter, *Angew. Chem., Int. Ed.* **2007**, *46*, 3706.
[23] M. H. Abraham, J. A. Platts, *J. Organ. Chem.* **2001**, *66*, 3484.
[24] A. Halabi, P. Froimowicz, M. C. Strumia, *Polym. Bull.* **2003**, *51*, 119.
[25] B. Dolenský, R. Konvalinka, M. Jakubek, V. Král, *J. Mol. Struct.* **2013**, *1035*, 124.
[26] D. E. Fagnani, M. J. Meese, K. A. Abboud, R. K. Castellano, *Angew. Chem., Int. Ed.* **2016**, *55*, 10726.
[27] B. Chenon, C. Sandorfy, *Can. J. Chem.* **1958**, *36*, 1181.
[28] W. Klemperer, M. W. Cronyn, A. H. Maki, G. C. Pimentel, *J. Am. Chem. Soc.* **1954**, *76*, 5846.
[29] D. T. McQuade, S. L. McKay, D. R. Powell, S. H. Gellman, *J. Am. Chem. Soc.* **1997**, *119*, 8528.
[30] M. Tariq, S. Hameed, I. H. Bechtold, A. J. Bortoluzzi, A. A. Merlo, *J. Mater. Chem. C* **2013**, *1*, 5583.
[31] P. van Mourik, B. Norder, S. J. Picken, *Liq. Cryst.* **2012**, *39*, 493.
[32] H. Ishida, Y. H. Lee, *Polymer* **2001**, *42*, 6971.
[33] H. Ishida, Y.-H. Lee, *J. Polym. Sci. Part B: Polym. Phys.* **2001**, *39*, 736.
[34] S. Zheng, H. Lü, Q. Guo, *Macromol. Chem. Phys.* **2004**, *205*, 1547.
[35] Y.-C. Su, W.-C. Chen, K.-l. Ou, F.-C. Chang, *Polymer* **2005**, *46*, 3758.
[36] J.-M. Huang, S.-J. Yang, *Polymer* **2005**, *46*, 8068.
[37] B. Kiskan, Y. Yagci, *Polymer* **2005**, *46*, 11690.
[38] H.-J. Chiu, R.-S. Tsai, J.-M. Huang, *e-Polymers*, **2010**, *10*, 75.
[39] H. Lü, S. Zheng, *Polymer* **2003**, *44*, 4689.
[40] A. Laobuthee, S. Chirachanchai, H. Ishida, K. Tashiro, *J. Am. Chem. Soc.* **2001**, *123*, 9947.
[41] S. Chirachanchai, A. Laobuthee, S. Phongtamrug, *J. Heterocycl. Chem.* **2009**, *46*, 714.